Available online at www.sciencedirect.com

ScienceDirect

Advances in Space Research 71 (2023) 4276–4287

ADVANCES IN SPACE RESEARCH (a COSPAR publication)

www.elsevier.com/locate/asr

Low-thrust rendezvous trajectory generation for multi-target active space debris removal using the RQ-Law

Sanjeev Narayanaswamy [a,*], Benjamin Wu [b], Philippe Ludivig [c], Frank Soboczenski [d], Karthik Venkataramani [1], Christopher J. Damaren [a]

[a] University of Toronto Institute for Aerospace Studies, 4925 Dufferin Street, Toronto, Ontario M3H 5T6, Canada
[b] National Astronomical Observatory of Japan, Mitaka, Tokyo 181-8588, Japan
[c] University of Luxembourg, 2 avenue de l'Université, L-4365 Esch-sur-Alzette, Luxembourg
[d] SPHES, King's College London, London SE1 1UL, United Kingdom

Received 14 April 2022; received in revised form 2 December 2022; accepted 26 December 2022
Available online 30 December 2022

Abstract

The problem of space debris must be addressed to avoid a cascading collision in the near future that would critically damage humanity's space assets and dependent terrestrial infrastructure. One method of meeting this challenge is to use a dedicated spacecraft to deorbit a series of prioritized debris. To avoid a large fuel requirement, electric spacecraft propulsion can be used, for which a multiple-rendezvous low-thrust trajectory is of interest. In this study, we develop such a trajectory for a predetermined subset of the Iridium 33 debris using a two-step procedure. First, the target rendezvous order is determined by using relevant distance metrics to approximate the transfer cost between debris objects. Next, the RQ-Law, a recently developed Lyapunov feedback control law for generating low-thrust rendezvous trajectories, is used to generate a trajectory that can take a spacecraft to each of the studied debris objects in the determined order. This method can be used to rapidly determine low-thrust multi-target multi-revolution rendezvous trajectories in the preliminary design stage for missions such as space debris removal and satellite servicing without requiring an initial guess.

Keywords: Low-thrust; Space debris; Spacecraft rendezvous trajectory

1. Introduction

Space debris can be defined as unwanted or defunct objects in space (primarily around the Earth) and it is problematic not only for geocentric missions but also for interplanetary spacecraft which have to traverse this debris field. As a result of the thousands of pieces of debris in Earth orbit, it is essential to predict and avoid collisions (DeMars et al., 2014). In Kessler and Cour-Palais (1978), there is a well-known prediction about a collision chain reaction that could be triggered once a critical number of debris is reached. To prevent this phenomenon, now known as the Kessler Syndrome, it has been found that the debris must be prioritized and removed at the rate of at least five pieces a year (Liou et al., 2010).

Several methods are currently being studied for active space debris removal. Some of these concepts include satellite-based, tether-based, and laser-based systems (Mark and Kamath, 2019). Of these different methods, our focus lies on satellite-based systems which require the rendezvous of a deorbiting spacecraft, often referred to as

* Corresponding author.
E-mail addresses: sanjeev.narayanaswamy@mail.utoronto.ca (S. Narayanaswamy), benwu.astro@gmail.com (B. Wu), philippe.ludivig.001@student.uni.lu (P. Ludivig), frank.soboczenski@kcl.ac.uk (F. Soboczenski), venkataramani.karthik@gmail.com (K. Venkataramani), damaren@utias.utoronto.ca (C.J. Damaren).
[1] Independent Researcher.

https://doi.org/10.1016/j.asr.2022.12.049
0273-1177/

the chaser, with a space debris object before the method of debris removal can be enacted (harpoon, net, etc.). As an example, the RemoveDEBRIS mission (Aglietti et al., 2020) successfully tested harpoon and net deployment separately on test targets in 2018. Another satellite-based deorbiting demonstration mission, ELSA-d (Blackerby et al., 2018), was launched in 2021 and uses a magnetic capture system.

In this work, we determine a low-thrust multiple rendezvous trajectory for a debris mitigation problem using the RQ-Law, a Lyapunov feedback control law (Narayanaswamy and Damaren, 2023). First a background of the approaches to trajectory determination for space debris removal is given in Section 2. Then the methodology will be given in Section 3, where the debris mitigation scenario, target sequence analysis, trajectory generation method, and deorbiter spacecraft mass estimation will be presented. In Section 4, implementation details surrounding the code architecture and selected parameters will be provided. Finally, the conclusion will be given in Section 5.

2. Background & previous work

To achieve higher rates of annual debris removal while keeping the fuel mass requirement manageable, multiple-target low-thrust debris deorbiting missions are of interest (Braun et al., 2013). The generation of multi-target rendezvous trajectories can be broadly divided into two steps: 1) determining the order in which the targets must be visited and 2) finding a trajectory that connects these targets in the desired order. The sequencing of the targets is typically treated as a combinatorial optimization problem where computationally inexpensive metrics are used to characterize the transfer costs to each of the objects (Izzo and Simões, 2018). In particular, the traveling salesperson problem and its application to space debris, has been studied by Izzo et al. (2015) as well as Cerf (2013). However these works do not focus on the use of continuous low-thrust transfers with ion thrusters, but rather assume that the transfers are performed using impulsive chemical thrusters. In contrast, other studies are notable for analyzing debris sequencing for low-thrust rendezvous trajectories (Zhao et al., 2017; Olympio and Frouvelle, 2014; Barbee, 2012; Zuiani and Vasile, 2012; Di Carlo et al., 2017).

The next step of connecting these targets involves determining low-thrust geocentric rendezvous trajectories between each pair of objects in the sequence. Several studies have investigated this in the context of orbital debris removal and the closely related objective of satellite servicing. The analytical approach has found interest in the design of rendezvous trajectories to geostationary satellites (Bucci and Lavagna, 2016; Zhang et al., 2018; Han et al., 2019). Hakima and Emami (2019) used a Lyapunov guidance law for concurrent orbit and attitude control of an underactuated spacecraft and demonstrated its use for short-range rendezvous. Olympio and Frouvelle (2014) used an indirect method to design rendezvous trajectories for debris in sun-synchronous orbits. Zuiani and Vasile (2012) as well as Jorgensen and Sharf (2020) used the direct method for finding multiple-rendezvous trajectories to debris. Mei et al. (2021) applied the Legendre-Gauss–Lobatto pseudospectral direct collocation method (Garg et al., 2010; Narayanaswamy and Damaren, 2020) to find geostationary debris removal trajectories using solar sails. Leomanni et al. (2020) employed a Lyapunov guidance scheme for orbit raising and a model predictive controller for terminal rendezvous.

3. Methodology

3.1. Multiple debris deorbiting scenario

The scenario studied in this work is based upon the Orbital Debris Remediation Challenge (ODRC) proposed by the NASA Frontier Development Lab (Mackintosh, 2018). The goal is to design a trajectory that enables a debris deorbiting spacecraft (DDS) to rendezvous with a subset of 12 pieces of orbital debris from the Iridium 33 satellite (Liou and Shoots, 2009). Table 1 contains the orbital elements of the DDS and the chosen set of Iridium 33 debris objects. We see that each of the 12 debris objects and the DDS are in nearly polar, prograde ($1.5011\ \text{rad} \leqslant i \leqslant 1.5082\ \text{rad}$), close to circular ($e < 0.02$), Low Earth Orbits (LEO, $a \approx r_{Earth} + 622\ \text{km}$), with a range of Right Ascension of the Ascending Node (RAAN) values.

The primary trajectory design challenge is that the spacecraft is assumed to be equipped with a NEXT ion propulsion system with a maximum thrust of 0.236 N (Patterson and Benson, 2007). Upon each rendezvous, it releases a 1.2 kg capsule to attach onto that debris object. This capsule is modeled as a net combined with a passive deorbiting module such as the Terminator Tape^{TM}, that deploys a long conducting tape which decreases the orbital lifetime of the debris through electrodynamic and aerodynamic drag (Stankey and Hoyt, 2021). At the end of the mission, when the DDS exhausts its store of capsules, it will enter into a deorbiting trajectory itself, using passive means, to avoid adding to the space debris problem.

3.2. Target sequence order

The optimal sequence in which the DDS deorbits each debris object can be formulated as the solution to a variant of the traveling salesperson problem (TSP), a well-studied NP-hard problem in combinatorial optimization (Bui and Moon, 1994). Given a list of cities and their pairwise distances, the TSP seeks to find the minimum total distance of a route that passes through each city exactly once and returns to the starting location (Bye et al., 2021). More formally, as discussed by Izzo et al. (2015), given a complete graph $\mathcal{G} := \{\mathcal{V}, \mathbf{W}\}$, such that $\mathcal{V}$ is the set containing the vertices (cities) and $\mathbf{W} := \mathcal{V} \times \mathcal{V} \rightarrow \mathbb{R}^+$ is a map that asso-

Table 1
Initial orbital elements of the ODRC objects.

Object - Index	a [m]	e	i [rad]	ω [rad]	Ω [rad]	θ [rad]
DDS - 0	7164040.5518	0.0019	1.5079	0.8909	2.8765	5.3923
Debris - 1	6989199.3166	0.0030	1.5081	2.1655	2.6417	1.8687
Debris - 2	7148540.2308	0.0025	1.5081	1.0069	2.8457	5.3600
Debris - 3	7159283.7674	0.0017	1.5075	0.8765	2.7557	2.4102
Debris - 4	7163255.1260	0.0020	1.5082	1.0466	3.0286	2.0850
Debris - 5	7123773.3419	0.0020	1.5077	3.2640	2.6863	4.1132
Debris - 6	7105550.2633	0.0057	1.5027	3.1392	1.3450	5.1329
Debris - 7	7142543.1535	0.0033	1.5070	0.9020	2.5723	3.3631
Debris - 8	7312321.2253	0.0256	1.5011	2.1126	2.2211	0.9441
Debris - 9	7048230.6726	0.0019	1.5049	2.3550	1.0898	2.8958
Debris - 10	7078633.3020	0.0010	1.5068	3.8077	3.4273	2.3719
Debris - 11	6945287.2368	0.0021	1.5033	6.0589	0.1315	1.8640
Debris - 12	7127598.3265	0.0058	1.5070	0.4993	2.6333	1.5864

ciates each ordered vertex pair with a positive real number edge weight (distances between cities), the goal is to find the global minimum weight Hamiltonian path (route). Similar approaches relating the TSP to the problem of active orbital debris removal have been explored in the literature (Barbee, 2012; Cerf, 2013; Braun et al., 2013; Izzo et al., 2015). In the current work, the DDS takes the role of the salesperson, the debris objects are the cities, the final stop is unconstrained, and the relative distances change dynamically over time.

Determining a suitable distance metric is vital for properly mapping a problem to the TSP. In the case of orbital debris remediation, we set each edge distance to the orbital transfer energy. A large contribution to the transfer cost comes from the relative inclination, Δi, which can be calculated as:

$$\Delta i = \cos^{-1}(\cos i_1 \cos i_2 + \sin i_1 \sin i_2 \cos \Omega_1 \cos \Omega_2 + \sin i_1 \sin i_2 \sin \Omega_1 \sin \Omega_2), \quad (1)$$

where i is the inclination, Ω is the RAAN, and the subscripts denote the initial and final orbits, respectively (Izzo et al., 2015). We refer to this distance metric, Δi, as D_{Izzo}, and we note that it has units of radians.

Izzo et al. (2015) found that the optimal path calculated from D_{Izzo} is itself well-approximated by a simpler heuristic given by a Hamiltonian path of monotonically increasing Ω, or a "RAAN walk". We refer to this distance metric as $D_{\text{RAAN}} = \cos^{-1}(\cos(\Omega_2 - \Omega_1))$. Note that the true anomaly (θ; i.e., the position of the orbiting body along the ellipse at a specific time) is not included in this calculation as the contribution to orbital transfer energy is minimal. By choosing our distance metric in such a way, we transform the debris deorbiting problem from a dynamic TSP to a static TSP, making the solution much more tractable. The element θ is accounted for at a later stage during the rendezvous trajectory calculation.

Efficient computation of a TSP solution is an area of active research, with algorithms falling into two classes: exact and approximate (heuristic). An exhaustive search through all possible permutations leads to a solution of time order $\mathcal{O}((n-1)!)$, resulting in impractical computations for even modest sized graphs. Fortunately, the debris deorbiting problem presented in this work consists of 13 vertices (including the initial orbit of the DDS) and was solvable exactly within reasonable timescales (i.e., few hours on consumer-grade hardware). Nevertheless, for

Table 2
TSP-derived target sequences using D_{Izzo} as the transfer cost between each pair of targets. The normal distribution fits of the calculation times were calculated using ten samples for each method.

TSP Solver	Sequence	Average Calculation Time [s]	Standard Deviation of Calculation Time [s]	Max cost leg (cost [rad])	Total cost [rad]
Exact	[0, 4, 10, 2, 3, 5, 1, 12, 7, 8, 6, 9, 11]	2.320×10^{3}	4.369×10^{1}	9→11 (0.956)	3.838
Nearest Neighbor	[0, 2, 3, 5, 1, 12, 7, 8, 4, 10, 6, 9, 11]	2.690×10^{-4}	1.044×10^{-4}	10→6 (2.075)	5.143
Christofides	[0, 4, 10, 11, 9, 6, 8, 7, 12, 1, 5, 3, 2]	1.645×10^{-3}	3.830×10^{-4}	10→11 (2.939)	6.120
2-opt	[0, 4, 10, 11, 9, 6, 8, 7, 12, 1, 5, 3, 2]	2.723×10^{-3}	8.567×10^{-4}	10→11 (2.939)	6.120
3-opt	[0, 4, 10, 11, 9, 6, 8, 7, 12, 1, 5, 3, 2]	5.548×10^{-3}	7.770×10^{-4}	10→11 (2.939)	6.120
Lin-Kernighan	[0, 2, 3, 5, 1, 12, 7, 8, 6, 9, 11, 10, 4]	5.136×10^{-3}	5.040×10^{-4}	11→10 (2.939)	6.076
Simulated Annealing (Best of 500 runs)	[0, 2, 3, 5, 1, 12, 7, 8, 6, 9, 11, 10, 4]	1.648×10^{1}	4.984×10^{-1}	11→10 (2.939)	6.076

points of comparison and to explore future scalability, we applied 6 additional heuristic algorithms: nearest neighbor, Christofides (Christofides, 1976), 2-opt (Croes, 1958), 3-opt (Lin, 1965), Lin-Kernighan (Lin and Kernighan, 1973; Helsgaun, 2000), and simulated annealing (Kirkpatrick et al., 1983). The 2-opt and 3-opt use an initial solution from Christofides, while simulated annealing takes the best of 500 stochastic runs using an initial temperature parameter of 1 and a decrease factor of 0.95 over 1000 iterations. The resulting sequences and corresponding costs are shown in Table 2.

From these experiments, we found that none of the heuristic algorithms reached the global optimum solution of 3.838 rad. Of the approximate solvers used, the nearest neighbor approach found the lowest cost (5.143 rad), followed by Lin-Kernighan and simulated annealing (6.076 rad each). Christofides reached 6.120 rad and was not improved through the 2-opt and 3-opt local searches. The latter 5 methods each included the transfer to/from debris objects 10 and 11, leading to relatively expensive maximum transfer legs of 2.939 rad. Interestingly, we also see from the calculation time statistics in Table 2, that the nearest neighbor approach — which found the sequence with the lowest cost among the approximate methods investigated — happened to take the least amount of calculation time.

The experiment was repeated using the D_{RAAN} metric, which returned the same sequences for each respective algorithm as found using D_{Izzo}. Notably, the RAAN walk heuristic agreed with the exact sequence, outperforming the other heuristic algorithms tested. For our remaining trajectory analysis, we choose to use the final target sequence of $S_{\text{exact}} = [0, 4, 10, 2, 3, 5, 1, 12, 7, 8, 6, 9, 11]$.

3.3. RQ-Law

To determine rendezvous trajectories to each of the target debris objects, we will use the RQ-Law, a recently developed Lyapunov feedback control law for low-thrust multi-revolution rendezvous, which is described in detail in Narayanaswamy and Damaren (2023). This law is based on the Q-Law developed by Petropoulos (2005) and cast into an modified equinoctial framework by Varga and Pérez (2016). For convenience, we summarize here the primary elements of the RQ-Law.

The Lyapunov function that we will use takes the form

$$Q = \left(1 + W_P P\right) \sum_{\text{œ}} S_{\text{œ}} W_{\text{œ}} \left(\frac{\text{œ}_C - \text{œ}_{T,aug}}{\dot{\text{œ}}_{C,max,\alpha\beta L}} \right)^2, \quad \text{œ} \in \{a, f, g, h, k\} \tag{2}$$

where we note that the semi-major axis a is used instead of the semi-latus rectum, p, in the set of modified equinoctial elements, œ, and that Q has units of time squared (Varga and Pérez, 2016). We note that all the terms in the expression for Q are scalars and that the summation iterates over each œ in the set $\{a, f, g, h, k\}$. In addition, we state here that the RQ-Law has singularities corresponding to the classical orbital elements $e = 0, e = 1$, and $i = \pi$. The set œ_C corresponds to the orbital elements of the chaser, $W_{\text{œ}}$ are the associated scalar weights, and the quantity $\dot{\text{œ}}_{C,max,\alpha\beta L}$ represents the maximum rate of change for each chaser orbital element, œ_C, with respect to both thrust direction and true longitude. The quantity P is the penalty function, W_p is the associated weight, and $S_{\text{œ}}$ is the scaling function. These quantities, along with the expressions for $\dot{\text{œ}}_{C,max,\alpha\beta L}$, will be discussed later in more detail. The augmented set of target orbital elements, $\text{œ}_{T,aug}$, is defined as

$$\text{œ}_{T,aug} = \begin{cases} \frac{2W_L}{\pi}\left(a_T - \frac{r_{p,min}}{1-\sqrt{f_C^2+g_C^2}}\right) \\ \quad \times \tan^{-1}\left(W_{scl}\Delta L_{[-\pi,\pi]}\right) + a_T, & \text{œ} = a \\ \text{œ}_T, & \text{œ} \in \{f, g, h, k\} \end{cases} \tag{3}$$

where the set œ_T represents the unaugmented target orbital elements. The quantity $\Delta L_{[-\pi,\pi]} = L_C - L_T$, is the difference in radians between the true longitudes of the chaser and target wrapped to the range $[-\pi, \pi]$, $r_{p,min}$ is the minimum periapsis radius constraint, and W_L and W_{scl} are phasing parameters.

The RQ-Law operates over two stages. In Stage 1, $W_L = 0$ and the chaser's goal is to transfer to the same orbit as the target, matching all the target orbital elements except for L_T. In Stage 2, $W_L > 0$ and the chaser will try to match the phase of the moving target in order to achieve rendezvous.

The following expressions, $\dot{\text{œ}}_{max,\alpha\beta L}$, expressed in modified equinoctial elements for any maneuvering spacecraft, can be obtained from Varga and Pérez (2016):

$$\dot{a}_{max,\alpha\beta L} = 2Fa\sqrt{\frac{a}{\mu}}\sqrt{\frac{1+\sqrt{f^2+g^2}}{1-\sqrt{f^2+g^2}}} \tag{4}$$

$$\dot{f}_{max,\alpha\beta L} \approx 2F\sqrt{\frac{a\left(1-f^2-g^2\right)}{\mu}} \tag{5}$$

$$\dot{g}_{max,\alpha\beta L} \approx 2F\sqrt{\frac{a\left(1-f^2-g^2\right)}{\mu}} \tag{6}$$

$$\dot{h}_{max,\alpha\beta L} = \frac{1}{2}F\sqrt{\frac{a\left(1-f^2-g^2\right)}{\mu}}\frac{s^2}{\sqrt{1-g^2}+f} \tag{7}$$

$$\dot{k}_{max,\alpha\beta L} = \frac{1}{2}F\sqrt{\frac{a\left(1-f^2-g^2\right)}{\mu}}\frac{s^2}{\sqrt{1-f^2}+g} \tag{8}$$

where the given expressions for $\dot{f}_{max,\alpha\beta L}$ and $\dot{g}_{max,\alpha\beta L}$ are approximations, $s^2 = 1 + h^2 + k^2$, and F is the magnitude of the thrust-acceleration $\vec{\mathbf{F}} = \vec{\mathbf{T}}/m$, with $\vec{\mathbf{T}}$ being the thrust. As described in Narayanaswamy and Damaren (2023), the approximations for $\dot{f}_{max,\alpha\beta L}$ and $\dot{g}_{max,\alpha\beta L}$ presented in Eqs. (5) and (6) are inaccurate for certain orbits. To improve upon this, we used the equations given by Yuan et al. (2007) in Eqs. (9) and (10):

$$\dot{f}_{max,\alpha\beta} = \frac{F}{q}\sqrt{\frac{p}{\mu}}\sqrt{(f+\sin(L)(q+1))^2 + q^2\sin^2(L) + g^2(k\cos(L) - h\sin(L))^2} \tag{9}$$

$$\dot{g}_{max,\alpha\beta} = \frac{F}{q}\sqrt{\frac{p}{\mu}}\sqrt{(g+\sin(L)(q+1))^2 + q^2\cos^2(L) + f^2(k\cos(L) - h\sin(L))^2} \tag{10}$$

where $q = 1 + f\cos(L) + g\sin(L)$ and $p = a\left(1 - f^2 - g^2\right)$. It is important to note that Eqs. (9) and (10) only give the maximal rates of change over the thrust angles. Using a mesh of 100 true longitude values in $[0, 2\pi]$, we can numerically approximate the values of $L_{C,max,\dot{f}}$ and $L_{C,max,\dot{g}}$ that maximize $\dot{f}_{max,\alpha\beta}$ and $\dot{g}_{max,\alpha\beta}$, respectively.

The penalty function, P, is given by

$$P = \exp\left[k_{pen}\left(1 - \frac{r_{p,C}}{r_{p,min}}\right)\right] \tag{11}$$

and this helps to make the minimum radius of the chaser spacecraft, $r_{p,C} = a_C(1 - e_C)$, stay above a specified $r_{p,min}$. The scalar k_{pen}, and as mentioned earlier, W_p, are weights associated with this penalty function. The scaling function $S_{\text{œ}}$ can be written as

$$S_{\text{œ}} = \begin{cases} \left[1 + \left(\frac{|a_C - a_{T,aug}|}{m_{scl}a_{T,aug}}\right)^{n_{scl}}\right]^{1/r_{scl}}, & \text{œ} = a \\ 1, & \text{œ} \in \{f, g, h, k\} \end{cases} \tag{12}$$

where the quantities m_{scl}, n_{scl}, and r_{scl} are associated scalar weights.

For a spacecraft equipped with a constant-thrust engine, the in-plane and out-of-plane Lyapunov-optimal thrust angles, α^* and β^*, need to be found such that whenever the thrusters are active, $\dot{Q}$, the rate of change of the Lyapunov function, is minimized. The thrust angles are defined in the Local-Vertical-Local-Horizontal (LVLH) frame $\mathcal{F}_{\underset{\rightarrow}{LVLH}} = \left[\frac{\underset{\rightarrow}{\mathbf{r}}}{|\underset{\rightarrow}{\mathbf{r}}|} \quad \frac{\underset{\rightarrow}{\mathbf{h}} \times \underset{\rightarrow}{\mathbf{r}}}{|\underset{\rightarrow}{\mathbf{h}} \times \underset{\rightarrow}{\mathbf{r}}|} \quad \frac{\underset{\rightarrow}{\mathbf{h}}}{|\underset{\rightarrow}{\mathbf{h}}|}\right]^T$ attached to the chaser spacecraft. In the definition of $\mathcal{F}_{\underset{\rightarrow}{LVLH}}$, $\underset{\rightarrow}{\mathbf{r}}$ and $\underset{\rightarrow}{\mathbf{h}}$ are the orbital position and orbital angular momentum vectors, respectively. The thrust-acceleration $\underset{\rightarrow}{\mathbf{F}}$ is related to the thrust angles α and β via

$$\underset{\rightarrow}{\mathbf{F}} = \begin{bmatrix} F_r \\ F_\theta \\ F_h \end{bmatrix} = \begin{bmatrix} F\cos\beta\sin\alpha \\ F\cos\beta\cos\alpha \\ F\sin\beta \end{bmatrix} \tag{13}$$

Numerical propagation of the nonlinear dynamics of a spacecraft using modified equinoctial elements can be done using Gauss' variational equations (Varga and Pérez, 2016):

$$\begin{bmatrix} \dot{a} \\ \dot{f} \\ \dot{g} \\ \dot{h} \\ \dot{k} \\ \dot{L} \end{bmatrix} = \mathbf{A}\begin{bmatrix} F_r \\ F_\theta \\ F_h \end{bmatrix} + \mathbf{b} \tag{14}$$

where the matrix $\mathbf{A}$ and column vector $\mathbf{b}$ are expressed as

$$\mathbf{A} = \frac{1}{q}\sqrt{\frac{a\left(1-f^2-g^2\right)}{\mu}}\begin{bmatrix} \frac{2aq(f\sin(L) - g\cos(L))}{1-f^2-g^2} & \frac{2aq^2}{1-f^2-g^2} & 0 \\ q\sin(L) & (q+1)\cos(L) + f & -g(h\sin(L) - k\cos(L)) \\ -q\cos(L) & (q+1)\sin(L) + g & f(h\sin(L) - k\cos(L)) \\ 0 & 0 & \frac{\cos(L)}{2}\left(1 + h^2 + k^2\right) \\ 0 & 0 & \frac{\sin(L)}{2}\left(1 + h^2 + k^2\right) \\ 0 & 0 & h\sin(L) - k\cos(L) \end{bmatrix} \tag{15}$$

$$\mathbf{b} = \begin{bmatrix} 0 & 0 & 0 & 0 & 0 & \frac{q^2\sqrt{a\mu\left(1-f^2-g^2\right)}}{a^2\left(1-f^2-g^2\right)^2} \end{bmatrix}^T \tag{16}$$

with

$$q = 1 + f\cos(L) + g\sin(L) \tag{17}$$

The expressions for the Lyapunov-optimal thrust angles can be expressed as $\alpha^* = \arctan(-D_2, -D_1)$ and $\beta^* = \arctan\left(\frac{-D_3}{\sqrt{D_1^2+D_2^2}}\right)$ where the two-argument arctangent is used for finding α^*. The D_i are defined as

$$D_1 = \sum_{oe}\left(\frac{\partial Q}{\partial oe_C} + \frac{\partial Q}{\partial \dot{f}_{C,max,\alpha\beta L}}\frac{\partial \dot{f}_{C,max,\alpha\beta L}}{\partial oe_C} + \frac{\partial Q}{\partial \dot{g}_{C,max,\alpha\beta L}}\frac{\partial \dot{g}_{C,max,\alpha\beta L}}{\partial oe_C}\right)\frac{\partial \dot{oe}_C}{\partial F_\theta} \tag{18}$$

$$D_2 = \sum_{oe}\left(\frac{\partial Q}{\partial oe_C} + \frac{\partial Q}{\partial \dot{f}_{C,max,\alpha\beta L}}\frac{\partial \dot{f}_{C,max,\alpha\beta L}}{\partial oe_C} + \frac{\partial Q}{\partial \dot{g}_{C,max,\alpha\beta L}}\frac{\partial \dot{g}_{C,max,\alpha\beta L}}{\partial oe_C}\right)\frac{\partial \dot{oe}_C}{\partial F_r} \tag{19}$$

$$D_3 = \sum_{oe}\left(\frac{\partial Q}{\partial oe_C} + \frac{\partial Q}{\partial \dot{f}_{C,max,\alpha\beta L}}\frac{\partial \dot{f}_{C,max,\alpha\beta L}}{\partial oe_C} + \frac{\partial Q}{\partial \dot{g}_{C,max,\alpha\beta L}}\frac{\partial \dot{g}_{C,max,\alpha\beta L}}{\partial oe_C}\right)\frac{\partial \dot{oe}_C}{\partial F_h} + \frac{\partial Q}{\partial L_C}A_{C,(6,3)} \tag{20}$$

where $A_{C,(6,3)}$ refers to the (6,3) component in Eq. (15) for the chaser spacecraft.

Table 3
Mass breakdown of NEXT ion thruster system (Patterson and Benson, 2007).

NEXT Ion Thruster Component	Mass [kg]
Ion Thruster	13.5
Gimbal	6
Power Management System	5
Power Processing Unit	34.5
Total	**59**

We also adopt the notion of relative effectivity, η_r, to create a coasting mechanism (Petropoulos, 2005). This is defined as $\eta_r = \frac{\dot{Q}_n - \dot{Q}_{nx}}{\dot{Q}_{nn} - \dot{Q}_{nx}}$, where $\dot{Q}_n$ is the Lyapunov-optimal value of $\dot{Q}$ at the current time t and

$$\dot{Q}_{nn} = \min_{[t,t+T]}\dot{Q}_n \tag{21}$$

$$\dot{Q}_{nx} = \max_{[t,t+T]}\dot{Q}_n \tag{22}$$

The quantities $\dot{Q}_{nn}$ and $\dot{Q}_{nx}$ represent the minimum and maximum values of $\dot{Q}_n$, respectively, that could occur in the current osculating orbit of the chaser, with period T. If $\eta_r \geqslant \eta_{r,tol}$, where $\eta_{r,tol}$ is some set threshold value, then the propulsion system for the chaser is turned on. Otherwise, the spacecraft is allowed to coast, trading a higher time of flight for a lower fuel consumption. The integration is terminated when the relative position error and relative velocity errors with respect to the target are less than some specified tolerances $r_{err,tol}$ and $v_{err,tol}$.

3.4. Deorbiter spacecraft mass estimation

To create an approximate mass budget for our Debris Deorbiter Spacecraft (DDS), we first examined the driving factors. Unlike most spacecraft operating in LEO, which use their propulsion systems for orbit adjustment early in their mission and for infrequent stationkeeping thereafter, the DDS spends most of its mission changing its orbit in order to rendezvous with debris. Therefore, the mass allocations for the propellant as well as the propulsion subsystem need to be higher to reflect this.

The NEXT ion thruster, which uses Xenon fuel, was chosen for the DDS since it has a high maximum thrust

Table 4
Mass budget for the DDS spacecraft compared with a mass budget from a 14.75 kg debris deorbiter CubeSat (Hakima et al., 2018) and a mass budget composed of averages from various Low Earth Orbit spacecraft equipped with a propulsion subsystem (Wertz et al., 2011). All percentages are relative to wet mass.

Subsystem	Debris Deorbiter Spacecraft (DDS) - (Mass [kg])	Debris Deorbiter Spacecraft (DDS)	Reference A (Hakima et al., 2018)	Reference B (Wertz et al., 2011)
Payload	14.4	2.06%	0.00%	24.41%
Structure and Mechanisms	135.0	19.29%	20.00%	21.26%
Thermal Control	11.0	1.57%	-	1.57%
Power	83.0	11.86%	9.00%	16.54%
Telemetry, Tracking, and Command	7.0	1.00%	1.00%	1.57%
Onboard Processing	7.0	1.00%	1.00%	3.94%
Attitude Determination and Control	47.0	6.71%	10.00%	4.72%
Propulsion	59.0	8.43%	10.70%	2.36%
Other	7.0	1.00%	1.00%	2.36%
Dry Mass (not incl. payload)	356.0	50.86%	52.70%	54.33%
Total Dry Mass (incl. payload)	370.4	52.92%	52.70%	78.74%
Propellant	329.6	47.08%	47.30%	21.26%
Wet Mass (Total Dry Mass + Propellant)	700.0	100.00%	100.00%	100.00%

of 276 mN for an ion thruster with a high specific impulse of 4170 s (Patterson and Benson, 2007). Although the combination of high thrust and specific impulse values for this engine allow fuel-efficient changes to the spacecraft orbit, the power consumption is also large (7 kW). In terms of flight heritage, the recently launched Double Asteroid Redirection Test (DART) mission is equipped with a NEXT ion thruster (Cheng et al., 2020). From Patterson and Benson (2007), we can determine the mass of a single NEXT thruster with its supporting systems to be 59 kg, as seen in Table 3. To determine the wet mass of the DDS, ratios of wet mass (m_0) to thruster power (P) were calculated using representative values given in Kluever and Oleson (1998). It was seen that these were in the range $m_0/P = [90, 183]$ with units kg/kW. Taking a value of $m_0/P = 100$ kg/kW, and knowing that the NEXT engine consumes 7kW at its maximum thrust, this indicates that $m_0 = 700$ kg is a reasonable estimate for the DDS wet mass.

To determine the dry mass and propellant allocation for the DDS, two reference mass budgets are used, which are given in Table 4. Reference A is from a debris deorbiter CubeSat designed by Hakima et al. (2018). Since the mission is similar to that of the DDS in the current research, the mass budget from that paper was taken as the primary reference. We note that in Reference A, the payload allocation is zero since the deorbiter CubeSat attaches onto a debris object and enters into a deorbiting trajectory, unlike the DDS, which releases a 1.2 kg capsule to deorbit each debris object. Since the mass of the CubeSat in Reference A is 14.75 kg while the wet mass of the DDS is 700 kg, an additional reference is needed to justify scaling the mass allocations to a much larger wet mass. For this reason, we used subsystem mass allocations averaged across a variety of LEO spacecraft of different sizes equipped with propulsion subsystems from Wertz et al. (2011), denoted as Reference B. It can be seen that the biggest differences are in the mass allocations for the propulsion, power, and payload subsystems as well as for the propellant. As expected, a larger allocation for propulsion and propellant are needed for the DDS since most of its mission involves changing orbits. Since the DDS payload consists of the twelve deorbiting capsules, while the payloads of most LEO spacecraft involve an observation or communications instrument with a significant power draw, the payload and power requirements are smaller compared to Reference B. In addition, we note that a separate mass allocation for Thermal Control was not given in Reference A, most probably due to being included in the Structure and Mechanisms subsystem, so the value from Reference B is used instead for the DDS. For the other subsystems we see that the mass allocations for the DDS are similar to the averages given in Reference B for LEO spacecraft. From this we can see that the dry mass for the DDS is 370.4 kg, which gives a Xenon propellant allocation of 329.6 kg.

4. Implementation

4.1. Code architecture

The bulk of the RQ-Law implementation has been written in C++ for computational efficiency using the Armadillo linear algebra library (Sanderson and Curtin, 2016) with a top-level script implemented in MATLAB^{TM} that serves as a user interface. The problem parameters can be specified in this main script, which will then compile and call the various C++ files. Since the full expressions for Q and D_i are quite unwieldy, a description of the RQ-Law was first written symbolically and then converted into a C++ function. The open source CVODE solver, published by the Lawrence Livermore National Laboratory as part of the SUNDIALS suite, is used as the adaptive numerical integrator for its ability to handle stiff systems and for its support of event detection (Hindmarsh et al., 2005).

4.2. Event detection for orbit acquisition and rendezvous

The rendezvous trajectory is separated into the orbit acquisition stage (Stage 1) and the target acquisition stage (Stage 2) as discussed in Section 3.3. This also agrees with the recommendation of Naasz in his analysis of mean motion control (Naasz, 2002). In Stage 1, $W_L = 0$ and the chaser will match all of the target orbital elements except for L_T. In Stage 2, $W_L > 0$, and the chaser will perform phasing in order to achieve rendezvous with the target. In order to detect the termination of each stage, the event detection functionality in CVODE is used, which searches for roots of user specified functions (Hindmarsh et al., 2005).

For the RQ-Law, the functions used for determining the termination of Stage 1 and Stage 2, respectively, are:

$$\psi_{Stage1} = \begin{bmatrix} -1 \\ Q - Q_{tol} \end{bmatrix} \tag{23}$$

$$\psi_{Stage2} = \begin{bmatrix} \Delta L_{[-\pi,\pi]} \\ \max((r_{err} - r_{err,tol}), (v_{err} - v_{err,tol})) \end{bmatrix} \tag{24}$$

In each stage, CVODE is set to search for roots of both components of ψ, but termination will only occur when the second component is zero. For Stage 1, the chaser is considered to be on the same orbit as the target when $Q = Q_{tol}$. For Stage 2, rendezvous is considered to have occurred when $r_{err} \leqslant r_{err,tol}$ and $v_{err} \leqslant v_{err,tol}$. In Stage 1, roots of $Q - Q_{tol}$ are relatively easy to bracket since the first five orbital elements, $\{a, f, g, h, k\}$, which contribute to Q during orbit acquisition, are not expected to change significantly once the chaser transfers onto the target orbit. In contrast, in Stage 2, the roots of the function $\max((r_{err} - r_{err,tol}), (v_{err} - v_{err,tol}))$ are much more difficult to bracket since the relative position and velocity error tolerances required for rendezvous will only be satisfied for a brief period of time. If the step size chosen by the integrator

Table 5
Physical parameters for multiple rendezvous trajectory generation.

Initial Mass m_0 [kg]	Propellant Mass m_{fuel} [kg]	Capsule Mass [kg]	Thrust Magnitude $\lvert\vec{\mathbf{T}}\rvert$ [N]	Specific Impulse I_{sp} [s]	Standard Gravity g_0 $[\mathrm{m/s^2}]$	Initial Time t_0 [s]	Standard Gravitational Parameter μ $[\mathrm{m^3/s^2}]$	Earth Radius R_{Earth} [m]	Distance Scaling Unit DU [m]	Time Scaling Unit TU [s]
700	329.6	1.2	0.236	4170	9.81	0	3.9860×10^{14}	6.3781×10^{6}	R_{Earth}	$\sqrt{R_{Earth}^3/\mu}$

is too large, there is a chance that the rendezvous event would be missed if the second component of ψ_{Stage2} is positive on either side of the timestep.

For this reason, the first component of ψ_{Stage2}, is used as an auxiliary in determining the roots of the second component of ψ_{Stage2}. The function $\Delta L_{[-\pi,\pi]}$, which is $(L_C - L_T)$ wrapped to the range $[-\pi, \pi]$, has easily bracketable roots of odd multiplicity. Since $\Delta L_{[-\pi,\pi]} = 0$ is a necessary condition for rendezvous, by forcing CVODE to also search for roots of this function, it will take smaller time steps in the vicinity of the desired roots of the second component of ψ_{Stage2} as well. Due to the ease with which the roots of $Q - Q_{tol}$ are found, it was not deemed necessary to introduce such an auxiliary function for Stage 1 and therefore the first component of ψ_{Stage1} was set to -1.

4.3. Rendezvous trajectory generation

Here we design a rendezvous trajectory in Low Earth Orbit by implementing the RQ-Law described in Section 3.3. The physical parameters used are in Table 5. Canonical scaling units of $DU = R_{Earth}$ and $TU = \sqrt{R_{Earth}^3/\mu}$ are used such that the scaled standard gravitational parameter is unity. These physical parameters correspond to a chaser spacecraft equipped with a NEXT ion thruster and 1.2 kg deorbiting capsules as described in Section 3.1. The parameters for the RQ-Law (Narayanaswamy and Damaren, 2023) were chosen through a combination of problem-specific tuning and reference to prior work (Lantukh et al., 2017; Petropoulos, 2005), and are listed in Table 6. The rendezvous conditions were chosen to be $r_{err,tol} = 1$ m and $v_{err,tol} = 1.5$ m/s. Relative and absolute integration tolerances of 1×10^{-7} are used with the CVODE adaptive numerical integrator. We note that the initial conditions in Table 1 are displayed in the form of classical orbital elements for ease of interpretation but are converted to modified equinoctial elements internally to use with the RQ-Law.

Based on the parameters in Tables 5 and 6, a rendezvous trajectory that reaches 8 of the 12 debris objects mentioned in Table 1, using the available fuel, is shown in Figs. 1 and 2. The rendezvous sequence, $S = [0, 4, 10, 2, 3, 5, 1, 12, 7]$, corresponds to a subset of the exact sequence discussed in Section 3.2. It can be seen from Figs. 1 and 2d that the RAAN values for the targets, which are the primary differences among the orbital elements of the target debris, are sequentially reached by the chaser. From Fig. 2a we see that the RQ-Law commands the semi-major axis to increase in order to make the RAAN changes more efficient. This is an inherited property from the Q-Law, upon which the RQ-Law is based, since the maximal rate of change of the RAAN is higher at larger semi-major axis values (Hatten, 2012). The rendezvous conditions of $r_{err,tol} = 1$ m and $v_{err,tol} = 1.5$ m/s are met for each target, as seen in Figs. 2h and 2i. The non-constant rate of change of the chaser mass, as seen in Fig. 2j, is due to the engine coasting as a result of the relative effectivity feature. The instantaneous changes in mass at the rendezvous times

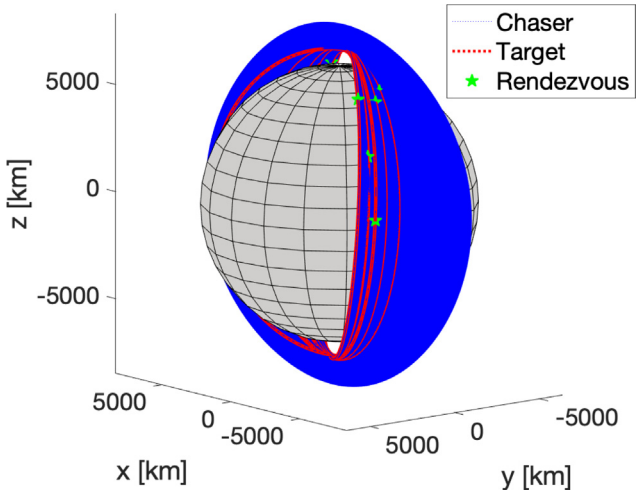

Fig. 1. Low-thrust multiple rendezvous trajectory.

Table 6
RQ-Law parameters for multiple rendezvous trajectory generation.

Stage	k_{pen}	$r_{p,min}$	W_p	W_a	W_f	W_g	W_h	W_k	W_{scl}	W_L	m_{scl}	n_{scl}	r_{scl}	$\eta_{r,tol}$	$r_{err,tol}$ [m]	$v_{err,tol}$ [m/s]	Q_{tol}
Stage 1	100	R_{Earth}	1	2	50	50	1	1	0	0	3	4	2	0.7	N/A	N/A	1×10^{-3}
Stage 2	100	R_{Earth}	1	10	1	1	1	1	0.7	6×10^{-2}	3	4	2	0	1	1.5	N/A

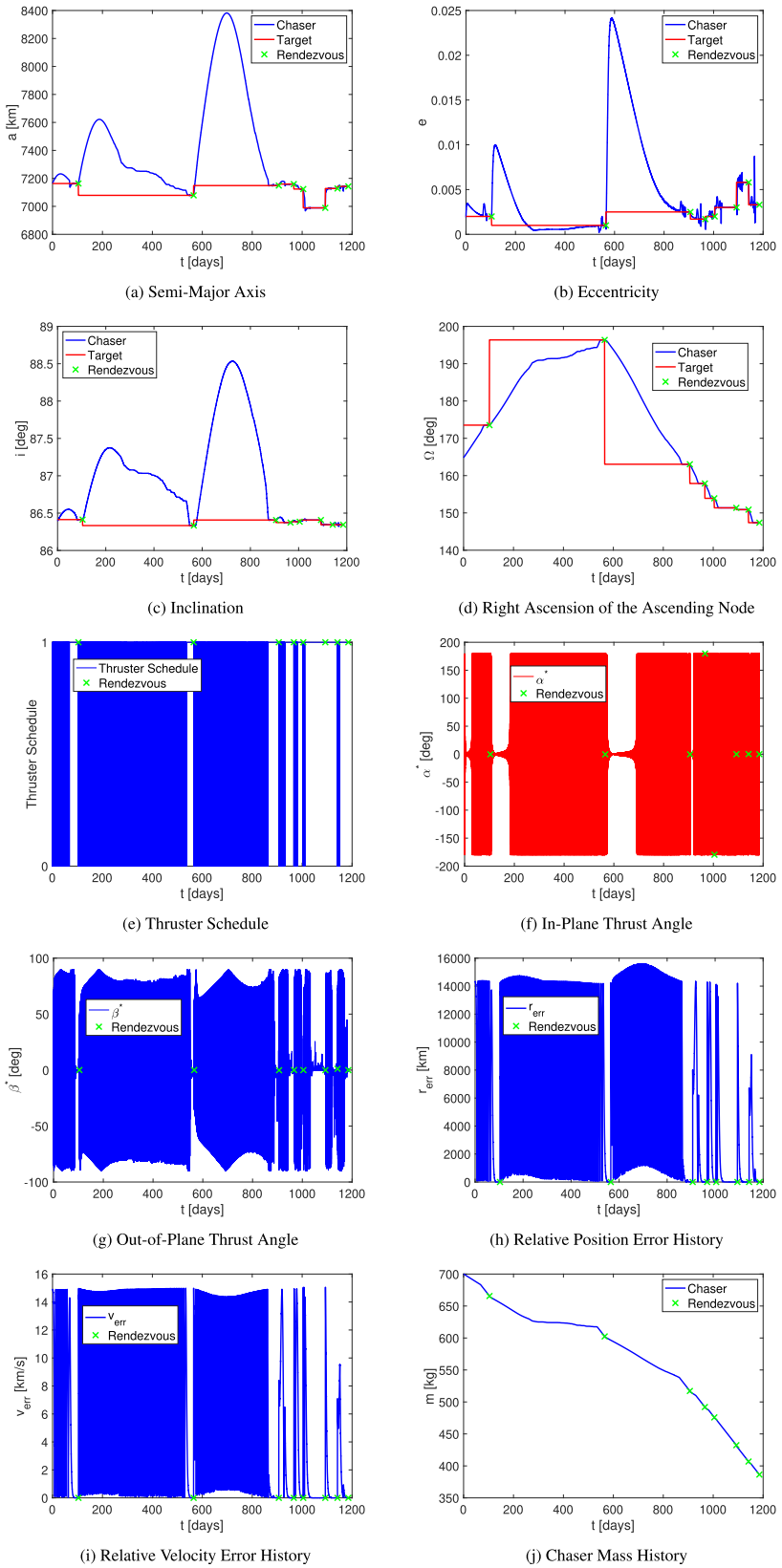

(a) Semi-Major Axis

(b) Eccentricity

(c) Inclination

(d) Right Ascension of the Ascending Node

(e) Thruster Schedule

(f) In-Plane Thrust Angle

(g) Out-of-Plane Thrust Angle

(h) Relative Position Error History

(i) Relative Velocity Error History

(j) Chaser Mass History

Fig. 2. Low-thrust multiple rendezvous trajectory - supporting plots.

model the deorbiting capsule deployment. The thruster schedule can be seen in Fig. 2e, where the seemingly solid blocks of color show rapid switching of the engine. The total fuel consumption is 305.2 kg and the total transfer time is 1185 days.

5. Conclusion

Through the use of the RQ-Law, a Lyapunov feedback control law capable of generating low-thrust rendezvous trajectories to moving targets, a multiple debris deorbiting trajectory has been found. First we split the problem of multiple low-thrust rendezvous into two parts: target sequence determination and trajectory generation. Two orbital transfer cost metrics, based on relative inclination and the RAAN difference, respectively, were used to determine the least expensive target sequence. Because we transformed this multiple debris rendezvous problem into a static TSP, we were able to find the global optimum sequence through a brute force search using both the RAAN difference metric and the relative inclination metric. Although it was found that the brute force search performed better than several TSP heuristic algorithms, our analysis and comparison of these heuristic algorithms may be relevant when scaling to more complex problems with a larger number of debris. Using the determined target order, we applied the RQ-Law to generate low-thrust trajectories to enable the debris deorbiting spacecraft to sequentially rendezvous with each debris object. Based on the available propellant and other mission parameters, the determined end-to-end trajectory is shown to successfully rendezvous with 8 debris objects from the larger set of 12 objects considered for analysis. The mission duration is around 3 years, which is primarily due to the large dispersal in RAAN values. However, it should be noted that only a small subset of the Iridium 33 debris cloud was considered for this analysis and if all the space debris surrounding the Earth is considered in aggregate, then trajectories that meet or exceed the recommended annual deorbital rate of 5 prioritized debris objects (Liou et al., 2010) are likely possible.

The multiple-rendezvous trajectories generated by this approach are intended for rapid iterations in the preliminary design stage. To obtain more accurate results, these trajectories can be used as initial guesses for higher fidelity methods, such as pseudospectral methods, that can include perturbative effects in the dynamics. Some perturbative effects that can be studied in future analyses, as a part of these higher fidelity methods, are the J_2 perturbation (due to Earth's oblateness) and atmospheric drag. Due to the generality of this approach, the method of first determining the target order followed by rendezvous trajectory generation using the RQ-Law can also be used for satellite servicing missions in addition to space debris removal. In this sense, the propellant onboard the DDS can also be considered part of the payload, in addition to the debris deorbiting capsules. If a fleet of DDS are considered, then this opens up the possibility of sharing fuel in order to increase the total number of debris and/or spacecraft reached.

Declaration of Competing Interest

The authors declare that they have no known competing financial interests or personal relationships that could have appeared to influence the work reported in this paper.

Acknowledgments

The authors would like to thank Graham Mackintosh of NASA FDL for creating the AI Challenge for Orbital Debris Remediation, which motivated our research into this topic. We are grateful to Chit Hong Yam of ispace Inc. and Stefano Campagnola of NASA JPL, who first suggested we look into the Q-Law literature. We also thank Dario Izzo of ESA ACT, Luís F. Simões of ML Analytics, Michael Saunders of Stanford University, and Philip Gill of University of California, San Diego for valuable discussions. We would like to acknowledge the use of the Niagara supercomputer at the University of Toronto (Ponce et al., 2019). Finally, the authors are grateful for support from the Ontario Graduate Scholarship, the Natural Sciences and Engineering Research Council of Canada (Grant Number RGPIN-2020-04037), a Grant-in-Aid for Scientific Research (KAKENHI Number 20K14706) of the Japan Society for the Promotion of Science (JSPS), and the Luxembourg National Research Fund (FNR Grant No. 11824057).

References

Aglietti, G.S., Taylor, B., Fellowes, S., Salmon, T., Retat, I., Hall, A., Chabot, T., Pisseloup, A., Cox, C., Zarkesh, A., Mafficini, A., Vinkoff, N., Bashford, K., Bernal, C., Chaumette, F., Pollini, A., Steyn, W.H., 2020. The active space debris removal mission RemoveDebris. Part 2: In orbit operations. Acta Astronaut. 168, 310–322. https://doi.org/10.1016/j.actaastro.2019.09.001.

Barbee, B.W.A., 2012. Design of Spacecraft Missions to Remove Multiple Orbital Debris Objects. In: 35th Annual AAS Guidance and Control Conference. Breckenridge, CO, United States.

Blackerby, C., Okamoto, A., Fujimoto, K., Okada, N., Forshaw, J.L., Auburn, J., 2018. ELSA-D: An In-Orbit End-Of-Life Demonstration Mission. In: 69th International Astronautical Congress. Bremen, Germany. p. 7.

Braun, V., Lüpken, A., Flegel, S., Gelhaus, J., Möckel, M., Kebschull, C., Wiedemann, C., Vörsmann, P., 2013. Active debris removal of multiple priority targets. Adv. Space Res. 51 (9), 1638–1648. https://doi.org/10.1016/j.asr.2012.12.003.

Bucci, L., Lavagna, M.R., 2016. Analytical Formulation for Light and Fast Low-Thrust Guidance Design to Perform Multi-Target On-Orbit Servicing. In: AIAA Guidance, Navigation, and Control Conference. American Institute of Aeronautics and Astronautics, San Diego, California, USA. https://doi.org/10.2514/6.2016-0877.

Bui, T., Moon, B., 1994. A new genetic approach for the traveling salesman problem. In: Proceedings of the First IEEE Conference on Evolutionary Computation. IEEE World Congress on Computational Intelligence. IEEE, Orlando, FL, USA, pp. 7–12. https://doi.org/10.1109/ICEC.1994.350051.

Bye, R.T., Gribbestad, M., Chandra, R., Osen, O.L., 2021. A Comparison of GA Crossover and Mutation Methods for the Traveling Salesman Problem. In: Innovations in Computational Intelligence and Computer Vision. Springer, pp. 529–542.

Cerf, M., 2013. Multiple Space Debris Collecting Mission—Debris Selection and Trajectory Optimization. J. Optim. Theory Appl. 156 (3), 761–796. https://doi.org/10.1007/s10957-012-0130-6.

Cheng, A.F., Stickle, A.M., Fahnestock, E.G., Dotto, E., Della Corte, V., Chabot, N.L., Rivkin, A.S., 2020. DART mission determination of momentum transfer: Model of ejecta plume observations. Icarus 352, 113989. https://doi.org/10.1016/j.icarus.2020.113989.

Christofides, N., 1976. Worst-case analysis of a new heuristic for the travelling salesman problem. Technical Report Carnegie-Mellon Univ Pittsburgh Pa Management Sciences Research Group.

Croes, G.A., 1958. A method for solving traveling-salesman problems. Oper. Res. 6 (6), 791–812, URL http://www.jstor.org/stable/167074.

DeMars, K.J., Cheng, Y., Jah, M.K., 2014. Collision Probability with Gaussian Mixture Orbit Uncertainty. J. Guidance Control Dyn. 37 (3), 979–985. https://doi.org/10.2514/1.62308.

Di Carlo, M., Romero Martin, J.M., Vasile, M., 2017. Automatic trajectory planning for low-thrust active removal mission in low-earth orbit. Adv. Space Res. 59 (5), 1234–1258. https://doi.org/10.1016/j.asr.2016.11.033.

Garg, D., Patterson, M., Hager, W.W., Rao, A.V., Benson, D.A., Huntington, G.T., 2010. A unified framework for the numerical solution of optimal control problems using pseudospectral methods. Automatica 46 (11), 1843–1851.

Hakima, H., Emami, M.R., 2019. Concurrent attitude and orbit control for Deorbiter CubeSats. Aerosp. Sci. Technol. 97, 105616. https://doi.org/10.1016/j.ast.2019.105616.

Hakima, H., Bazzocchi, M.C.F., Emami, M.R., 2018. A deorbiter CubeSat for active orbital debris removal. Adv. Space Res. 61 (9), 2377–2392. https://doi.org/10.1016/j.asr.2018.02.021.

Han, C., Zhang, S., Wang, X., 2019. On-orbit servicing of geosynchronous satellites based on low-thrust transfers considering perturbations. Acta Astronaut. 159, 658–675. https://doi.org/10.1016/j.actaastro.2019.01.041.

Hatten, N.A., 2012. A Critical Evaluation of Modern Low-Thrust, Feedback-Driven Spacecraft Control Laws. M.S. Thesis University of Texas.

Helsgaun, K., 2000. An effective implementation of the Lin–Kernighan traveling salesman heuristic. Eur. J. Oper. Res. 126(1), 106–130. URL: https://doi.org/10.1016/S0377-2217(99)00284-2.

Hindmarsh, A.C., Brown, P.N., Grant, K.E., Lee, S.L., Serban, R., Shumaker, D.E., Woodward, C.S., 2005. SUNDIALS: Suite of nonlinear and differential/algebraic equation solvers. ACM Trans. Mathe. Softw. (TOMS) 31 (3), 363–396. https://doi.org/10.1145/1089014.1089020.

Izzo, D., Simões, L.F., 2018. Acta Futura, Issue 11. Zenodo. https://doi.org/10.5281/zenodo.1142858.

Izzo, D., Getzner, I., Hennes, D., Simões, L.F., 2015. Evolving Solutions to TSP Variants for Active Space Debris Removal. In Proceedings of the 2015 Annual Conference on Genetic and Evolutionary Computation - GECCO '15. ACM Press, Madrid, Spain, pp. 1207–1214. https://doi.org/10.1145/2739480.2754727.

Jorgensen, M.K., Sharf, I., 2020. Optimal planning for a multiple space debris removal mission using high-accuracy low-thrust transfers. Acta Astronaut. 172, 56–69. https://doi.org/10.1016/j.actaastro.2020.03.031.

Kessler, D.J., Cour-Palais, B.G., 1978. Collision frequency of artificial satellites: The creation of a debris belt. J. Geophys. Res.: Space Phys. 83 (A6), 2637–2646. https://doi.org/10.1029/JA083iA06p02637.

Kirkpatrick, S., Gelatt, C.D., Vecchi, M.P., 1983. Optimization by simulated annealing. Science, 220(4598), 671–680. URL: https://doi.org/10.1126/science.220.4598.671.

Kluever, C.A., Oleson, S.R., 1998. Direct approach for computing near-optimal low-thrust earth-orbit transfers. J. Spacecraft Rockets 35 (4), 509–515. https://doi.org/10.2514/2.3360.

Lantukh, D.V., Ranieri, C.L., DiPrinzio, M.D., Edelman, P.J., 2017. Enhanced Q-Law Lyapunov Control for Low-Thrust Transfer and Rendezvous Design. In: 2017 AAS/AIAA Astrodynamics Specialist Conference.

Leomanni, M., Bianchini, G., Garulli, A., Giannitrapani, A., Quartullo, R., 2020. Orbit control techniques for space debris removal missions using electric propulsion. J. Guidance Control Dyn. 43 (7), 1259–1268. https://doi.org/10.2514/1.G004735.

Lin, S., 1965. Computer solutions of the traveling salesman problem. Bell Syst. Techn. J. 44(10), 2245–2269. URL: https://doi.org/10.1002/j.1538-7305.1965.tb04146.x.

Lin, S., Kernighan, B.W., 1973. An effective heuristic algorithm for the traveling-salesman problem. Oper. Res. 21 (2), 498–516, URL: http://www.jstor.org/stable/169020.

Liou, J.C., Shoots, D., 2009. Satellite collision leaves significant debris clouds. Orbital Debris Quart. News 13 (2), 1.

Liou, J.C., Johnson, N.L., Hill, N.M., 2010. Controlling the growth of future LEO debris populations with active debris removal. Acta Astronaut. 66 (5), 648–653. https://doi.org/10.1016/j.actaastro.2009.08.005.

Mackintosh, G., 2018. AI Challenge for Orbital Debris Remediation. Technical Report NASA Frontier Development Laboratory.

Mark, C.P., Kamath, S., 2019. Review of active space debris removal methods. Space Policy 47, 194–206. https://doi.org/10.1016/j.spacepol.2018.12.005.

Mei, H., Damaren, C.J., Zhan, X., 2021. Feedback pseudospectral method for end-of-life geostationary satellites removal using solar sailing. J. Guidance Control Dyn., 1–10 https://doi.org/10.2514/1.G005631.

Naasz, B.J., 2002. Classical Element Feedback Control for Spacecraft Orbital Maneuvers. M.S. Thesis Virginia Tech.

Narayanaswamy, S., Damaren, C.J., 2023. Equinoctial Lyapunov control law for low-thrust rendezvous. J. Guidance Control Dyn. https://doi.org/10.2514/1.G006662.

Narayanaswamy, S., Damaren, C.J., 2020. Comparison of the Legendre-Gauss pseudospectral and Hermite–Legendre–Gauss–Lobatto methods for low-thrust spacecraft trajectory optimization. Aerospace Syst. 3 (1), 53–70. https://doi.org/10.1007/s42401-019-00042-w.

Olympio, J., Frouvelle, N., 2014. Space debris selection and optimal guidance for removal in the SSO with low-thrust propulsion. Acta Astronaut. 99, 263–275. https://doi.org/10.1016/j.actaastro.2014.03.005.

Patterson, M., Benson, S., 2007. NEXT Ion Propulsion System Development Status and Performance. In: 43rd AIAA/ASME/SAE/ASEE Joint Propulsion Conference & Exhibit. American Institute of Aeronautics and Astronautics, Cincinnati, OH. https://doi.org/10.2514/6.2007-5199.

Petropoulos, A.E., 2005. Refinements to the Q-law for low-thrust orbit transfers. In: 15th AAS/AIAA Space Flight Mechanics Conference. Copper Mountain, Colorado.

Ponce, M., van Zon, R., Northrup, S., Gruner, D., Chen, J., Ertinaz, F., Fedoseev, A., Groer, L., Mao, F., Mundim, B.C., Nolta, M., Pinto, J., Saldarriaga, M., Slavnic, V., Spence, E., Yu, C.-H., Peltier, W.R., 2019. Deploying a Top-100 Supercomputer for Large Parallel Workloads: The Niagara Supercomputer. In: Proceedings of the Practice and Experience in Advanced Research Computing on Rise of the Machines (Learning). ACM, Chicago IL USA, pp. 1–8. https://doi.org/10.1145/3332186.3332195.

Sanderson, C., Curtin, R., 2016. Armadillo: A template-based C++ library for linear algebra. J. Open Source Softw. 1 (2), 26. https://doi.org/10.21105/joss.00026.

Stankey, H.C., Hoyt, R.P., 2021. In-Flight Performance of the Terminator Tape End-of-Life Deorbit Module. In: Proceedings of the AIAA/USU Conference on Small Satellites. Logan, UT.

Varga, G.I., Pérez, J.M.S., 2016. Many-revolution low-thrust orbit transfer computation using equinoctial Q-law including J2 and eclipse effects. In: Advances in the Astronautical Sciences. Vail, United States volume 156. pp. 2463–2481.

Wertz, J.R., Everett, D.F., Puschell, J.J., 2011. Space Mission Engineering: The New SMAD. Microcosm Press.

Yuan, R., Pingyuan, C., Enjie, L., 2007. A low-thrust guidance law based on Lyapunov feedback control and hybrid genetic algorithm. Aircraft Eng. Aerospace Technol. 79 (2), 144–149. https://doi.org/10.1108/00022660710732699.

Zhang, S., Han, C., Sun, X., 2018. New solution for rendezvous between geosynchronous satellites using low thrust. J. Guidance Control Dyn. 41 (6), 1397–1406. https://doi.org/10.2514/1.G003270.

Zhao, S., Zhang, J., Xiang, K., Qi, R., 2017. Target sequence optimization for multiple debris rendezvous using low thrust based on characteristics of SSO. Astrodynamics 1 (1), 85–99. https://doi.org/10.1007/s42064-017-0007-4.

Zuiani, F., Vasile, M., 2012. Preliminary design of debris removal missions by means of simplified models for low-thrust, many-revolution transfers. Int. J. Aerospace Eng. 2012, 1–22. https://doi.org/10.1155/2012/836250.